PROCEEDINGS OF SPIE

SPIEDigitalLibrary.org/conference-proceedings-of-spie

Evolution of roughness during the pattern transfer of high-chi, 10nm half-pitch, silicon-containing block copolymer structures

Gregory Blachut, Stephen M. Sirard, Andrew Liang, Chris A. Mack, Michael J. Maher, et al.

Gregory Blachut, Stephen M. Sirard, Andrew Liang, Chris A. Mack, Michael J. Maher, Paulina A. Rincon-Delgadillo, Boon Teik Chan, Geert Mannaert, Geert Vandenberghe, C. Grant Willson, Christopher J. Ellison, Diane Hymes, "Evolution of roughness during the pattern transfer of high-chi, 10nm half-pitch, silicon-containing block copolymer structures," Proc. SPIE 10589, Advanced Etch Technology for Nanopatterning VII, 1058907 (22 March 2018); doi: 10.1117/12.2297489

SPIE.

Event: SPIE Advanced Lithography, 2018, San Jose, California, United States

Evolution of roughness during the pattern transfer of high-chi, 10 nm half-pitch, silicon-containing block copolymer structures

Gregory Blachut[*1], Stephen M. Sirard[1], Andrew Liang[1], Chris A. Mack[2], Michael J. Maher[3], Paulina A. Rincon-Delgadillo[4], Boon Teik Chan[4], Geert Mannaert[4], Geert Vandenberghe[4], C. Grant Willson[3], Christopher J. Ellison[5], Diane Hymes[1]

[1]Lam Research Corporation, 4650 Cushing Parkway, Fremont, California 94538, United States

[2]Fractilia, LLC, 1605 Watchhill Rd., Austin, TX 78703, United States

[3]McKetta Department of Chemical Engineering and Department of Chemistry, The University of Texas at Austin, Austin, Texas 78712, United States

[4]imec, Kapeldreef 75, 3001 Heverlee, Belgium

[5]Department of Chemical Engineering and Materials Science, The University of Minnesota—Twin Cities, 421 Washington Ave SE Rm 151, Minneapolis, Minnesota 55455, United States

ABSTRACT

A pattern transfer study was conducted to monitor the evolution of roughness in sub-10 nm half-pitch lines generated by the directed self-assembly (DSA) of a high-chi, silicon-containing block copolymer, poly(4-trimethylsilylstyrene)-*block*-poly(4-methoxystyrene). Unbiased roughness measurements were used to characterize the roughness of the structures before and after pattern transfer into silicon nitride. Parameters of the reactive ion etch process used as a dry development were systematically modified to minimize undesired line walking created by the DSA pre-pattern and to determine their impacts on roughness. The results of this study indicate that an optimized dry development can mitigate the effects of pre-pattern inhomogeneity, and that both dry development and pattern transfer steps effect the roughness of the final structures.

Keywords: block copolymers, directed self-assembly, high-chi, silicon-containing, roughness, pattern transfer

1. INTRODUCTION

The directed self-assembly (DSA) of block copolymers (BCP) offers a route to producing features with resolution far exceeding that of conventional lithography. Although defectivity remains a gating challenge for DSA introduction into semiconductor high-volume manufacturing, controlling the roughness in otherwise "well-aligned" BCP features is also necessary to meet manufacturing specifications. However, since the final roughness in a DSA pattern is an amalgam of roughness from the initial lithography, the pattern development and transfer, and the fluctuations inherent to self-assembly,[1] more work is required to understand the interplay of these various roughness sources.

The overwhelming majority of DSA research for line-space applications has utilized poly(styrene)-*block*-poly(methyl methacrylate) (PS-*b*-PMMA) as the BCP.[2–5] This material has the desirable property that at elevated annealing temperatures (~250°C), the two constituent polymers have approximately the same surface tension with air, avoiding the

[*]Corresponding author: greg.blachut@lamresearch.com

Advanced Etch Technology for Nanopatterning VII, edited by Sebastian U. Engelmann
Proc. of SPIE Vol. 10589, Tokyo Electron Ltd. 1058907 · © 2018 SPIE · CCC
code: 0277-786X/18/$18 · doi: 10.1117/12.2297489

formation of wetting layers and orienting the BCP domains perpendicularly to the surface, as needed for lithography.[6] Furthermore, the oxygen-containing PMMA block can be removed preferentially to the aromatic PS block with reactive ion etching (RIE), enabling facile process integration.[7] However, PS-*b*-PMMA suffers from a practical resolution limit of approximately 11 nm half pitch (HP).[8] This limit arises from the relatively low chemical incompatibility between the two polymers, often discussed in the context of the Flory-Huggins interaction parameter or χ (chi). In addition to enabling higher resolution, increasing χ has been predicted to improve roughness,[9] although χ is just one of many factors that may ultimately determine roughness.[1] Due to both improved scaling and the potential for improved roughness, there is an urgent push to evaluate so-called "high-χ" BCPs for DSA applications.

Silicon-containing BCPs are an example of high-χ BCPs being explored for DSA. Incorporating silicon into one block of a diblock copolymer enables the selective removal of the non-silicon block with an RIE and provides a route for forming a topographic etch mask with the BCP.[10,11] In addition, the modularity of silicon-containing BCPs allows tuning of parameters like chemical incompatibility,[12] ultimately producing high-χ values and enabling scaling to 5 nm HP.[13,14] The drawback to using silicon-containing BCPs is the need to prevent the formation of a wetting layer by the hydrophobic silicon-containing block at the air interface.[15] Recently, spin-coatable, polarity-switching topcoats[16,17] have been developed that are directly compatible with a variety of silicon-containing BCPs and DSA integration schemes,[18–20] enabling the use of silicon-containing BCPs to study high-χ DSA.

Dry development is the preferred method for transforming the BCP features into a topographic etch mask. Plasma processes are ubiquitous in manufacturing and enable straightforward integration with the rest of the wafer workflow. In addition, dry development circumvents pattern collapse observed with wet development,[2] an issue exacerbated by BCP feature scaling. However, the interactions between the BCP materials and the species produced by the plasma can be complicated.[11] Understanding what parameters of a RIE can change and improve the roughness characteristics of the final patterns produced by the DSA may be crucial to minimizing roughness, as has been discovered in the smoothing of conventional photoresists.[21]

The primary goal of this study is to investigate the roughness of DSA structures of a sub-10 nm HP, silicon-containing, high-χ BCP, poly(4-trimethylsilylstyrene)-*block*-poly(4-methoxystyrene) (PTMSS-*b*-PMOST), during dry development and pattern transfer. The pre-pattern used to align the BCP consists of guidestripes taller than the thickness of the background brush layer but shorter than the BCP layer thickness. This "hybrid" chemo-/grapho- epitaxy scheme was previously found to produce the highest quality of DSA without sacrificing areal density.[18,20] However, the inhomogeneity in the pre-pattern leads to a line walking issue with the baseline dry development processes, as the features in contact with the guidestripe etch differently than the features in contact with the brush. This undesirable behavior was largely corrected by optimizing the dry development process. We find that the sub-10 nm PTMSS-*b*-PMOST DSA features can be developed while maintaining relatively low line roughness and low line walk during the dry development, and that these improvements are maintained after pattern transfer.

2. EXPERIMENTAL

2.1 DSA wafer preparation

Wafers were prepared on an all-track process at imec as previously described.[22] The BCP used was a 19.6 nm full pitch poly(4-trimethylsilylstyrene)-*block*-poly(4-methoxystyrene) (PTMSS-*b*-PMOST). Characterization of the BCP and a description of the chemistries used to make the DSA pre-patterns have been previously published.[20] In short, an approximately 19 nm thick film of crosslinkable poly(2-vinylpyridine) (XP2VP) was coated on top of a 13 nm thick layer of silicon nitride and annealed under inert atmosphere to crosslink (note: previously, a crosslinkable poly(4-methoxystyrene) was used at this step). A 193i lithography step was then performed on the bilayer to print a matrix of line and space features at different pitches and CDs. The resist features were "trim etched" to simultaneously reduce the CD of the resist as well as to etch through the XP2VP to expose and oxidize the silicon nitride. After the resist was stripped, a layer of polymer brush (a hydroxyl-terminated random copolymer of polystyrene and poly(4-*tert*-butylstyrene)) was spin coated on top of the XP2VP to form an overburden. The wafer was annealed a second time to form an approximately 8 nm thick monolayer, ostensibly through a selective condensation reaction between the brush's hydroxyl terminus and the oxidized silicon nitride, and ungrafted brush was removed with solvent. Then the PTMSS-*b*-PMOST was spin coated to yield a film of approximately 33 nm, and then the topcoat was spin coated to yield a film of

approximately 20 nm on top of the BCP. The wafer was then annealed a third time to orient and align the BCP features. The topcoat was not removed before dry etching.

2.2 Etching

Wafers were cut into approximately 20 x 30 mm coupons, and the coupons were affixed to 300 mm resist carrier wafers with thermal paste. All samples were etched in a commercial 300 mm capacitively coupled plasma chamber from the Lam Research Flex® dielectric etch product line. Both oxidizing and reducing etch chemistries were used for dry development. For pattern transfer, a typical fluorine-containing etch for silicon nitride was used. Pattern transfer into silicon nitride occurred immediately after BCP dry development without breaking vacuum.

2.3 Inspection and metrology

Top-down micrographs were taken manually with a Hitachi CG4000 or CS4800 CD-SEM. Regions where the resist had been patterned with both 79 and 98 nm pitch structures (corresponding to 4x and 5x density multiplication), as well as CDs ranging from approximately 12 to 30 nm after trim etch, were inspected. Tilted and cross-sectional SEM images were taken with a ThermoFisher Scientific (formerly FEI) Verios 460L XHR SEM.

For roughness measurements, 15 rectangular micrographs with a 0.45 by 2.25 µm field of view were taken at locations on the chip corresponding to 79 nm pitch and 26 nm guidestripe CD (as measured after trim etch) for each set of conditions. On occasion, a dislocation defect was captured; these images were not saved and additional images were taken until 15 dislocation-free images were available. However, most features etched to the bottom of the film suffered from bridging defects. Although relatively sparse, it was not possible to consistently find fields without these defects, so they were included in the data set and no effort was made to exclude their influence from the roughness measurements. Edge detection, PSD creation, and roughness calculations of the SEM images was performed with MetroLER software (Fractilia, LLC).

3. RESULTS AND DISCUSSION

3.1 DSA mechanism

The film stack used in the DSA process and the final DSA pattern are shown in Figure 1. To create the DSA pattern, a modified version of the LiNe process was used.[23] The guidestripes and the backfill region, which constitute the chemical treatment layers on top of the silicon nitride underlayer, are composed of crosslinkable poly(2-vinylpyridine) (XP2VP) and polystyrene-*random*-poly(4-*tert*-butylstyrene), respectively. The PTMSS-*b*-PMOST BCP was deposited on top of these treatment layers, and last, a spin-coatable topcoat was applied to treat the top interface.

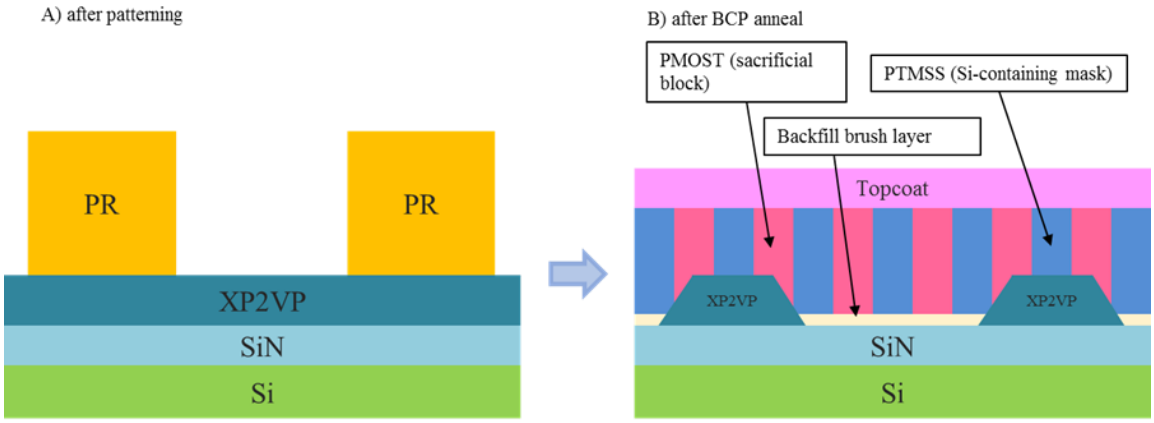

Figure 1. Schematic of a) filmstack after 193i patterning and b) filmstack after BCP anneal to form DSA patterns.

Note that in this process, the XP2VP is coated at a film thickness greater than that of the brush monolayer to produce topography in the chemical treatment layer. This was found to greatly improve the quality of DSA by reducing the number of dislocation defects, but significantly affects how the BCP aligns itself in relationship to the guidestripes. As depicted in Figure 1.B, it is believed that the hydrophobic PTMSS block – and not the more polar PMOST block – sits on top of the hydrophilic XP2VP guidestripe after DSA. This conclusion is supported by cross-sectional STEM EELS micrographs showing a silicon-rich domain sitting on top of the polar guidestripe in a similar process flow[20] (data explicitly showing the PTMSS on top of XP2VP will appear in a forthcoming publication). Further implicit evidence for this BCP arrangement on the guidestripe emerges in this publication, where line walking occurs with an odd number of domains; if the opposite PTMSS wetting situation was true, an even number of lines with distinct behavior would be anticipated due to symmetry. To explain this unexpected wetting behavior, the role of the sidewall edge of the guidestripe in DSA needs to be considered. During the trim etch which forms the guidestripe shape, the sidewall becomes highly polar due to the plasma, and the polarity is not significantly reduced during any of the subsequent process steps (resist strip, brush coat, brush anneal, or excess brush rinse).[24] When the BCP is finally coated and annealed on the DSA pre-pattern, the BCP arranges itself to minimize contact between the PTMSS and the polar sidewall, which places the PTMSS on *top* of the guidestripe due to the geometry of the pre-pattern. Because of this, for a set of four lines, exactly one PTMSS domain sits on top of the guidestripe, two domains sit on either side, and one domain sits completely in the backfill region without interfacing with the guidestripe. Again, the situation depicted in Figure 1.B creates significant inhomogeneity and presents an etch challenge.

3.2 Dry development

Both oxidizing and reducing RIEs are amenable to developing silicon-containing BCPs, like PTMSS-*b*-PMOST, by selectively removing the organic block.[11] To generate a baseline for the DSA structures, time splits of POR oxidizing and reducing dry development etch chemistries were performed with the goal of determining the time required to completely remove the sacrificial block and the underlying polymer treatment layers. Figure 2 shows the results of this time study. As these etch processes were known to develop this BCP's fingerprint patterns, it is unsurprising that both etches were effective at removing the PMOST on DSA patterns. The "100%" time point for each etch was selected as the sample where high-resolution tilted SEM imaging showed that the sacrificial PMOST block and the backfill brush had been completely removed and there was no evidence of scum in the interstitial regions. However, it is apparent that the features developed by either etch process are not uniform; one line periodically appears more distinct than its neighbors. For the oxidizing etch, the line walk manifests itself as a brighter line and is barely discernable in Figure 2.A (84%), but is readily apparent at the 100% and 140% time durations (Figures 2.B and 2.C). For the reducing etch process, the effect is not apparent at 50% etch time (Figure 2.D), faintly present at 100% etch time (Figure 2.E), and clearly present at 150% (Figure 2.F), appearing initially as line wiggling and then transforming into line collapse at 50% over-etch.

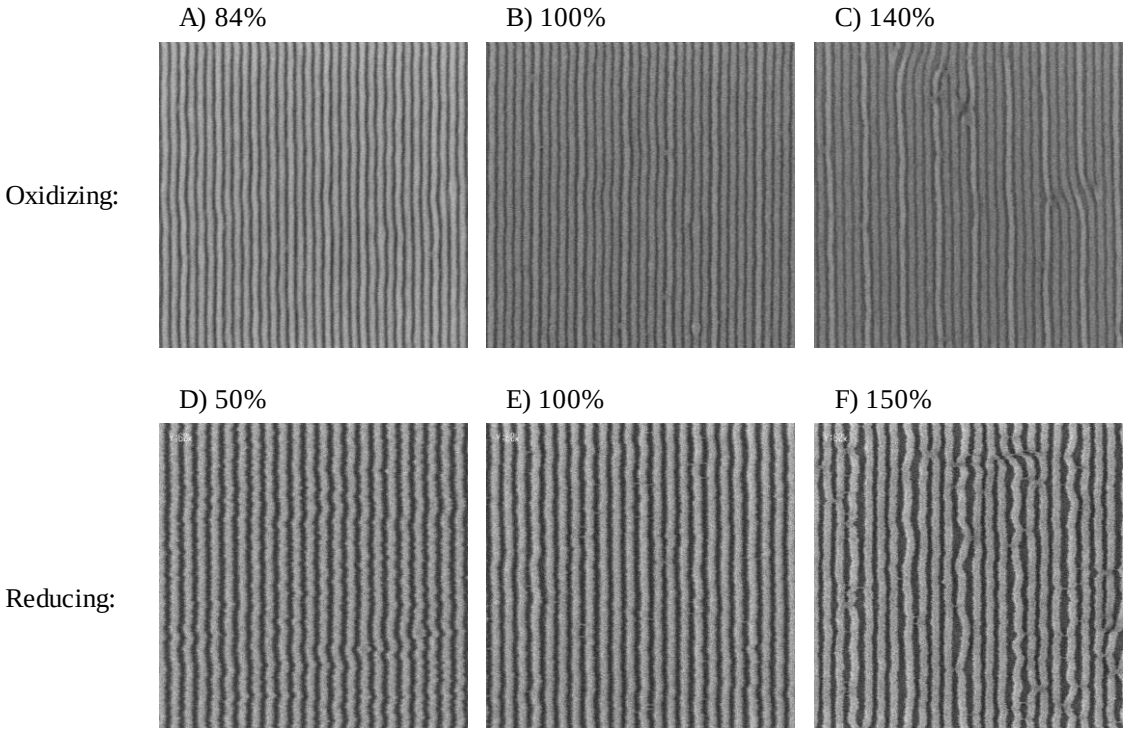

Figure 2. Dry developed features after oxidizing (top) and reducing (bottom) etch processes as a function of time (normalized to the time needed to fully remove the sacrificial material). The top images were each taken with a *square* 0.68 µm FoV scan, while the bottom images were each taken with a 0.45 by 2.25 µm FoV *rectangular* scan to exaggerate the line wiggling.

Since the line walk appears every fourth or fifth line depending on the pre-pattern pitch, and the other three or four lines appear nominally similar, it follows that the line walk occurs due to the inhomogeneity caused by the guidestripe in the pre-pattern. Furthermore, since the periodically different line looks different in the oxidizing etch than in the reducing etch, the phenomenon is dependent on the nature of the dry development chemistry.

Tilted SEM imaging reveals more about the structures after dry development and helps to produce plausible mechanisms. Figure 3 shows the features after the *longest* dry development for both the reducing and oxidizing etches.

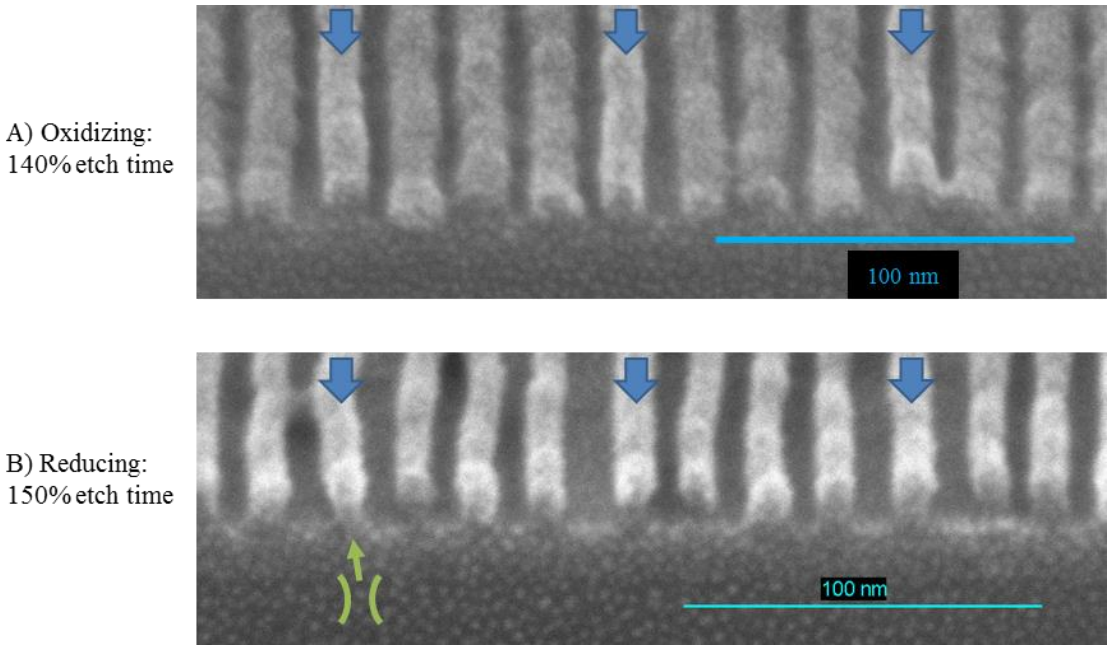

Figure 3. Tilted SEMs of A) 140% oxidizing etch time (Figure 2.C) and B) 150% reducing etch time (Figure 2.F). The three arrows at top each image of indicate the line walk and the arrow and cartoon on the bottom left-hand side indicate the guidestripe undercutting.

For the oxidizing chemistry, the micrograph shows that the distinct lines are taller and perhaps slightly thinner than the other lines (Figure 3.A). Recalling the alignment of the BCP on the topography as depicted in Figure 1.B, the conclusion to draw is that the feature that is a combination of the short Si-domain and the XP2VP guidestripe etches more slowly than the full-sized Si-domains alone with the oxidizing etch.

Conversely, the SEM of the reducing dry development (Figure 3.B) does not indicate that the geometry of the periodically unique line differs drastically from the other lines. Instead, just the bottom of the unique lines appears thinner, or undercut, especially when compared to the vertical profiles of the regular lines. This can be attributed to lateral etching of the guidestripe by the reducing process. Importantly, it does not appear that PTMSS on its own is as susceptible to lateral etching as is the guidestripe with the reducing chemistry. The observed line wiggle and line collapse can, therefore, be understood to be due to the diminished mechanical support specifically for the line sitting on the guidestripe.

To mitigate the line walk effects in the final DSA structures, a methodology to measure the extent of deviation was first developed. The MetroLER metrology software, used primarily to measure line roughness, was also used to calculate the average CD and pitch of each line, at a given position, for a set of micrographs. Figure 4, for example, shows the line-by-line average pitch deviation for the reducing RIE time split. Ideally, the line would be flat, indicating no positional dependence on pitch (or CD), but even at 50% time, where no pitch difference was visually discernable, the software detects periodic and predictable deviations for the lines. Furthermore, at 100% and 150% time duration, the differences evident by eye are readily quantified. Since both CD and pitch variation were observed, and are undesirable in the DSA features, the measured CD and pitch differences were combined to create a composite "line walk" metric to summarize the overall discrepancy between the two populations of lines. Physically, the line walk metric measures the combined CD and pitch deviation and would be zero for a set of identical lines, but does not discriminate between the two sources of deviation. Given the software's ability to measure seemingly imperceptible CD and pitch deviations, the use of the line walk metric to monitor feature deviation due to guidestripe effects was judged to be adequate to allow further process optimization.

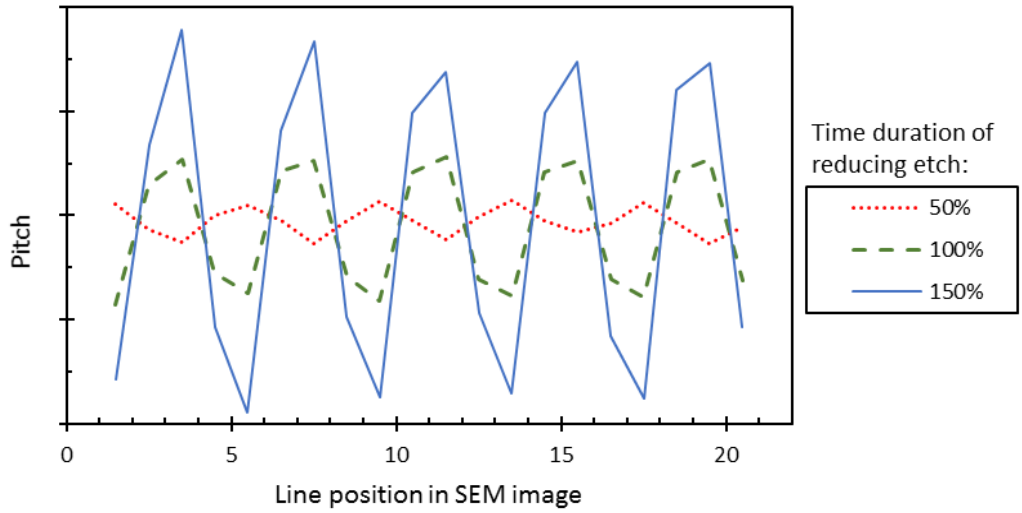

Figure 4. Average pitch between each line, for a given location in the SEM image, as a function of etch time for the reducing dry development.

To minimize the unwanted line walk effects, and to see the effect on roughness, a series of etch tests were performed where the process parameters of the reducing chemistry dry development were systematically varied. Both the roughness and the degree of CD/pitch walking, summarized as the line walk metric previously introduced, were measured. Figure 5 shows the results of the optimization study, where each point corresponds to the result of one set of RIE conditions. Compared to the baseline reducing etch, a modest 15% reduction in line edge roughness is possible, but more importantly, an almost 95% reduction in the line walk metric is observed. These results indicate that despite the chemical and topographic inhomogeneity in the DSA pre-pattern, it is possible to produce a highly uniform etch mask in the resultant DSA structures.

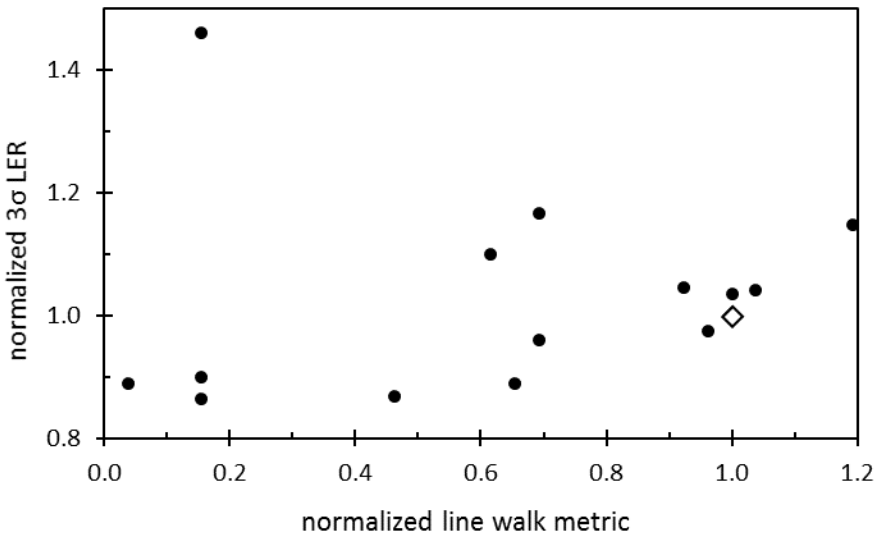

Figure 5. Normalized unbiased 3σ LER versus normalized line walk metric for the reducing dry development optimization study. Each point indicates the results from one set of RIE conditions. The diamond at (1,1) is the POR reducing process, which was used to normalize the data.

3.3 Pattern transfer

Pattern transfer of the features into the silicon nitride underlayer was then performed. Three different dry development conditions with different degrees of roughness and line walk were chosen for pattern transfer to better understand how each etch step affects the structures: the baseline reducing etch with low roughness and high line walk ("POR"), a set of conditions from the reducing etch split that gave high roughness but low line walk ("Rough"), and an optimized condition with low roughness and low pitch walk ("Optimized DD"). The three samples with different dry development conditions were then etched with the same silicon nitride etch chemistry. Figure 6 shows the line walk and the line edge roughness before and after pattern transfer for these samples. In general, the features after the silicon nitride etch process have increased line edge roughness and line walk, indicating the silicon nitride etch could be further optimized for this DSA hardmask. However, the large reduction line walk and the smaller reduction in roughness made possible by the optimized dry development remain present after the pattern transfer, indicating that the characteristics of the dry development etch are important for the overall quality of the resultant structures.

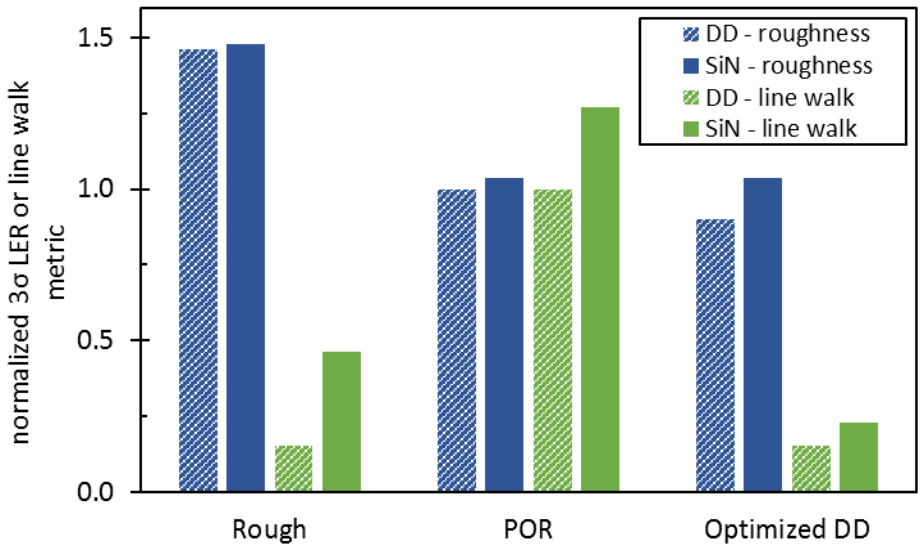

Figure 6. Summary of the line edge roughness and line walk after pattern transfer. The labels refer to which reducing dry development was used. Values are normalized to the baseline ("POR") dry development sample.

To confirm the pattern transfer, tilted and cross-sectional imaging was performed. Figure 7 shows the results from pattern transfer performed with the POR reducing dry development process. As can be seen, the features are etched into the silicon nitride underlayer without significant modification of the original structures. This shows that despite containing silicon, the PTMSS block can be used as an etch mask for silicon nitride.

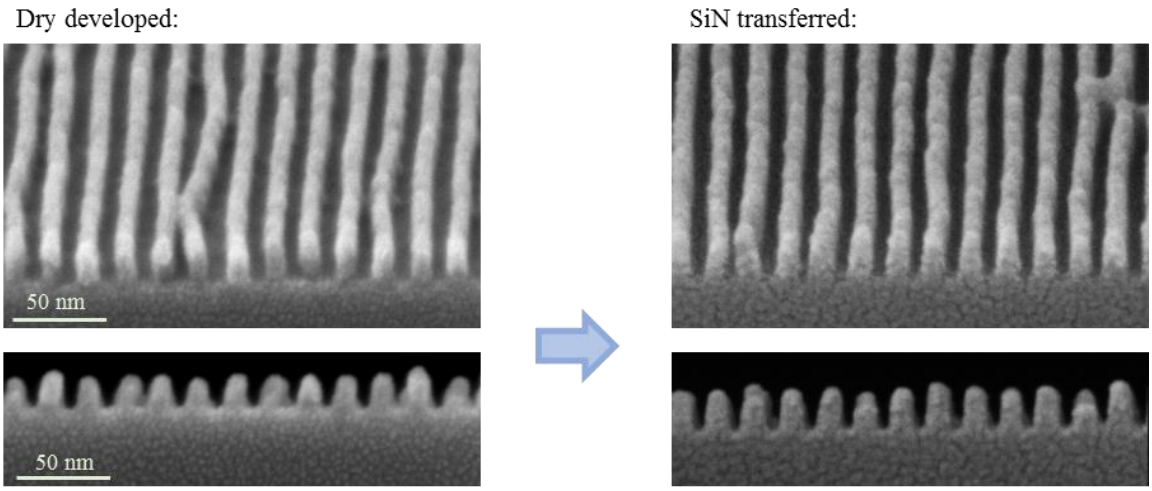

Figure 7. Tilted (top) and cross-sectional (bottom) SEMs of BCP features before and after pattern transfer into the 13 nm silicon nitride underlayer. These images were made using the unoptimized baseline reducing etch dry develop process, which suffers from line wiggle.

To further understand the evolution of roughness during the etch processes, power spectral density (PSD) curves of the LER after reducing dry development at 50% time duration, 100% time duration, and silicon nitride transfer were plotted and compared (Figure 8). The PSD curves are divided into low frequency (LF), mid frequency (MF), and high frequency (HF) regions, where each region has a characteristic slope and different factors contribute to roughness. Compared to the

50% time duration curve, the longer 100% time duration curve has lower roughness in the MF region and a higher overall correlation length, indicating the ability of the RIE to smooth the BCP lines on relatively short length-scales and reduce roughness. Although the 100% curve appears to have higher roughness than the 50% curve in the LF range, this may be due largely to the wiggling found only in the line that sits on the guidestripe, and not representative of the roughness in the correctly-behaving lines. Compared to the 100% POR etch, the roughness after the silicon nitride etch is slightly lower in the HF – an indication that this RIE step may also be smoothing the features – but noticeably higher across the rest of the frequencies; optimization of the silicon nitride etch with the DSA mask is expected to minimize this effect. In general, the fact that the roughness largely decreased from 50% to 100% time duration is encouraging since it indicates that the reducing RIE does not continuously degrade the pattern quality as dry development progresses, even taking into account the wiggling observed due to the guidestripe interaction.

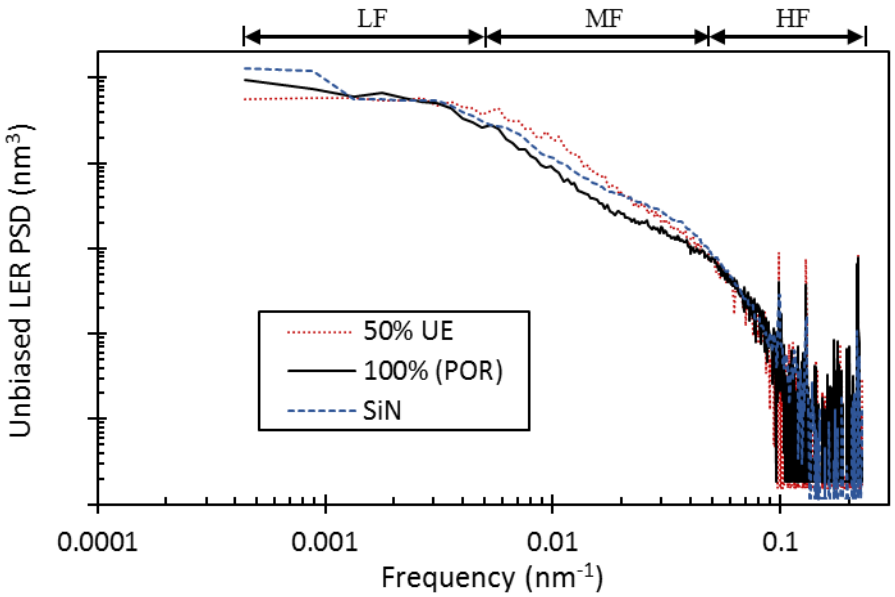

Figure 8: PSD curves of the unbiased line edge roughness of the features after POR reducing dry development etch at 50% under etch (UE), 100% etch time, and after transfer into the silicon nitride underlayer.

4. CONCLUSIONS

In summary, DSA patterns of a sub-10 nm HP sample of PTMSS-*b*-PMOST were etched and the roughness at various stages of the processes was measured. The tall guidestripe in the integration scheme, instrumental in reducing the defectivity of the DSA, unfortunately produces two populations of lines: the lines sitting on top of guidestripes and the lines sitting on the brush, and this pre-pattern inhomogeneity produced line walk during dry development. Of the two dry development RIEs screened, the reducing chemistry produced less severe line walk than the oxidizing chemistry on the DSA features. Further optimization of the reducing dry development largely mitigated the line walk issue and produced a slight improvement in roughness. After subsequent feature transfer into silicon nitride, an increase in both roughness and line walk was observed, but the optimization trends discovered for the dry development were maintained in the final structures. Optimization of the silicon nitride etch would likely to minimize these undesirable effects, but future pattern transfer studies should also audition different transfer layers that may be a better target for the PTMSS DSA mask.

Acknowledgements

The authors thank Dustin Janes for his help with preparing the wafers, the Lam Metrology team, and the Nanolab Technologies XSEM team.

REFERENCES

[1] Ruiz, R., Wan, L., Lopez, R. and Albrecht, T. R., "Line Roughness in Lamellae-Forming Block Copolymer Films," Macromolecules **50**(3), 1037–1046 (2017).

[2] Ruiz, R., Dobisz, E. and Albrecht, T. R., "Rectangular Patterns Using Block Copolymer Directed Assembly for High Bit Aspect Ratio Patterned Media," ACS Nano **5**(1), 79–84 (2011).

[3] Tsai, H., Pitera, J. W., Miyazoe, H., Bangsaruntip, S., Engelmann, S. U., Liu, C.-C., Cheng, J. Y., Bucchignano, J. J., Klaus, D. P., Joseph, E. A., Sanders, D. P., Colburn, M. E. and Guillorn, M. A., "Two-Dimensional Pattern Formation Using Graphoepitaxy of PS- *b* -PMMA Block Copolymers for Advanced FinFET Device and Circuit Fabrication," ACS Nano **8**(5), 5227–5232 (2014).

[4] Yang, X., Xiao, S., Hu, W., Hwu, J., van de Veerdonk, R., Wago, K., Lee, K. and Kuo, D., "Integration of nanoimprint lithography with block copolymer directed self-assembly for fabrication of a sub-20 nm template for bit-patterned media," Nanotechnology **25**(39), 395301 (2014).

[5] Pathangi, H., Chan, B. T., Bayana, H., Vandenbroeck, N., Heuvel, D. V. D., Look, L. V., Rincon-Delgadillo, P., Cao, Y., Kim, J., Lin, G., Parnell, D., Nafus, K., Harukawa, R., Chikashi, I., Polli, M., D'Urzo, L., Gronheid, R. and Nealey, P., "Defect mitigation and root cause studies in 14 nm half-pitch chemo-epitaxy directed self-assembly LiNe flow," J. MicroNanolithography MEMS MOEMS **14**(3), 031204 (2015).

[6] Mansky, P., "Controlling Polymer-Surface Interactions with Random Copolymer Brushes," Science **275**(5305), 1458–1460 (1997).

[7] Chan, B. T., Tahara, S., Parnell, D., Rincon Delgadillo, P. A., Gronheid, R., de Marneffe, J.-F., Xu, K., Nishimura, E. and Boullart, W., "28nm pitch of line/space pattern transfer into silicon substrates with chemo-epitaxy Directed Self-Assembly (DSA) process flow," Microelectron. Eng. **123**, 180–186 (2014).

[8] Wan, L., Ruiz, R., Gao, H., Patel, K. C., Albrecht, T. R., Yin, J., Kim, J., Cao, Y. and Lin, G., "The Limits of Lamellae-Forming PS- *b* -PMMA Block Copolymers for Lithography," ACS Nano **9**(7), 7506–7514 (2015).

[9] Bates, C. M., Maher, M. J., Janes, D. W., Ellison, C. J. and Willson, C. G., "Block Copolymer Lithography," Macromolecules **47**(1), 2–12 (2014).

[10] Azarnouche, L., Sirard, S. M., Durand, W. J., Blachut, G., Gurer, E., Hymes, D. J., Ellison, C. J., Willson, C. G. and Graves, D. B., "Plasma and photon interactions with organosilicon polymers for directed self-assembly patterning applications," J. Vac. Sci. Technol. B Nanotechnol. Microelectron. Mater. Process. Meas. Phenom. **34**(6), 061602 (2016).

[11] Sirard, S., Azarnouche, L., Gurer, E., Durand, W., Maher, M., Mori, K., Blachut, G., Janes, D., Asano, Y., Someya, Y., Hymes, D., Graves, D., Ellison, C. J. and Willson, C. G., "Interactions between plasma and block copolymers used in directed self-assembly patterning," 23 March 2016, 97820K.

[12] Durand, W. J., Blachut, G., Maher, M. J., Sirard, S., Tein, S., Carlson, M. C., Asano, Y., Zhou, S. X., Lane, A. P., Bates, C. M., Ellison, C. J. and Willson, C. G., "Design of high-χ block copolymers for lithography," J. Polym. Sci. Part Polym. Chem. **53**(2), 344–352 (2015).

[13] Cushen, J. D., Bates, C. M., Rausch, E. L., Dean, L. M., Zhou, S. X., Willson, C. G. and Ellison, C. J., "Thin Film Self-Assembly of Poly(trimethylsilylstyrene- *b* - D , L -lactide) with Sub-10 nm Domains," Macromolecules **45**(21), 8722–8728 (2012).

[14] Lane, A. P., Yang, X., Maher, M. J., Blachut, G., Asano, Y., Someya, Y., Mallavarapu, A., Sirard, S. M., Ellison, C. J. and Willson, C. G., "Directed Self-Assembly and Pattern Transfer of Five Nanometer Block Copolymer Lamellae," ACS Nano **11**(8), 7656–7665 (2017).

[15] Jung, Y. S. and Ross, C. A., "Orientation-Controlled Self-Assembled Nanolithography Using a Polystyrene−Polydimethylsiloxane Block Copolymer," Nano Lett. **7**(7), 2046–2050 (2007).

[16] Bates, C. M., Seshimo, T., Maher, M. J., Durand, W. J., Cushen, J. D., Dean, L. M., Blachut, G., Ellison, C. J. and Willson, C. G., "Polarity-Switching Top Coats Enable Orientation of Sub-10-nm Block Copolymer Domains," Science **338**(6108), 775–779 (2012).

[17] Maher, M. J., Bates, C. M., Blachut, G., Sirard, S., Self, J. L., Carlson, M. C., Dean, L. M., Cushen, J. D., Durand, W. J., Hayes, C. O., Ellison, C. J. and Willson, C. G., "Interfacial Design for Block Copolymer Thin Films," Chem. Mater. **26**(3), 1471–1479 (2014).
[18] Cushen, J., Wan, L., Blachut, G., Maher, M. J., Albrecht, T. R., Ellison, C. J., Willson, C. G. and Ruiz, R., "Double-Patterned Sidewall Directed Self-Assembly and Pattern Transfer of Sub-10 nm PTMSS- *b* -PMOST," ACS Appl. Mater. Interfaces **7**(24), 13476–13483 (2015).
[19] Maher, M. J., Rettner, C. T., Bates, C. M., Blachut, G., Carlson, M. C., Durand, W. J., Ellison, C. J., Sanders, D. P., Cheng, J. Y. and Willson, C. G., "Directed Self-Assembly of Silicon-Containing Block Copolymer Thin Films," ACS Appl. Mater. Interfaces **7**(5), 3323–3328 (2015).
[20] Blachut, G., Sirard, S. M., Maher, M. J., Asano, Y., Someya, Y., Lane, A. P., Durand, W. J., Bates, C. M., Dinhobl, A. M., Gronheid, R., Hymes, D., Ellison, C. J. and Willson, C. G., "A Hybrid Chemo-/Grapho-Epitaxial Alignment Strategy for Defect Reduction in Sub-10 nm Directed Self-Assembly of Silicon-Containing Block Copolymers," Chem. Mater. **28**(24), 8951–8961 (2016).
[21] Pargon, E., Azarnouche, L., Fouchier, M., Menguelti, K., Tiron, R., Sourd, C. and Joubert, O., "HBr Plasma Treatment Versus VUV Light Treatment to Improve 193 nm Photoresist Pattern Linewidth Roughness," Plasma Process. Polym. **8**(12), 1184–1195 (2011).
[22] Delgadillo, P. A. R., "Implementation of a chemo-epitaxy flow for directed self-assembly on 300-mm wafer processing equipment," J. MicroNanolithography MEMS MOEMS **11**(3), 031302 (2012).
[23] Liu, C.-C., Ramírez-Hernández, A., Han, E., Craig, G. S. W., Tada, Y., Yoshida, H., Kang, H., Ji, S., Gopalan, P., de Pablo, J. J. and Nealey, P. F., "Chemical Patterns for Directed Self-Assembly of Lamellae-Forming Block Copolymers with Density Multiplication of Features," Macromolecules **46**(4), 1415–1424 (2013).
[24] Williamson, L. D., Seidel, R. N., Chen, X., Suh, H. S., Rincon Delgadillo, P., Gronheid, R. and Nealey, P. F., "Three-Tone Chemical Patterns for Block Copolymer Directed Self-Assembly," ACS Appl. Mater. Interfaces **8**(4), 2704–2712 (2016).